Estimation of geometrical parameters and collimator evaluation for cone beam tomography

Grant T. Gullberg
Medical Imaging Research Laboratory, Department of Radiology, University of Utah, Salt Lake City, Utah 84132

Benjamin M. W. Tsui
Department of Radiology and Curriculum in Biomedical Engineering, University of North Carolina at Chapel Hill, Chapel Hill, North Carolina 27599

Carl R. Crawford
Applied Science Laboratory, GE Medical Systems, Milwaukee, Wisconsin 53201

J. Glen Ballard and John T. Hagius
Department of Radiology and Curriculum in Biomedical Engineering, University of North Carolina at Chapel Hill, Chapel Hill, North Carolina 27599

(Received 11 May 1989; accepted for publication 13 November 1989)

A method is presented for estimating the geometrical parameters for a cone beam detector geometry from the coordinates of the centroid of a projected point source sampled over 360°. Nonlinear expressions are derived for the coordinates of the centroids in terms of the geometrical parameters which include: the two-dimensional coordinates of the projection of the center of rotation onto the detector image plane; the focal length; the distance from the focal point to the center of rotation; and the spatial coordinates of the point source itself. Experimental data were obtained using a rotating gamma camera with a symmetrically converging collimator. The Marquardt algorithm was used to estimate the parameters for this particular cone beam geometry. The method was able to estimate the geometrical parameters and evaluate the accuracy of the collimator construction.

Key words: estimation, cone beam, collimator, single-photon emission computed tomography, x-ray computed tomography

I. INTRODUCTION

Today the rotating scintillation camera is the most widely used single-photon emission computed tomography (SPECT) system in clinical nuclear medicine. It has the advantage of being able to perform both body and brain SPECT imaging as well as conventional planar imaging. However, its sensitivity is less than optimum for imaging smaller organs such as the brain and the heart.

Steps have been taken to improve the sensitivity of SPECT imaging of smaller organs by utilizing fan beam collimators.[1-3] A multislice, short-bore fan-beam collimator that focuses to a line oriented parallel to the axis of rotation was originally developed for SPECT.[1] This was followed by a specially designed, long-bore fan-beam collimator for imaging the brain that would allow the face of the collimator to approach near the head and still allow the camera to clear the patient's shoulders.[3]

More recently, cone-beam collimation has been developed to optimize further the sensitivity of rotating camera SPECT systems.[4-8] Before this development, cone-beam collimation had been used for some time in nuclear medicine for planar imaging of small organs.[9-12] Two types of cone-beam geometries that have been utilized are the standard cone-beam collimator which consists of holes that converge to a single point behind the object, and the pin-hole collimator which has a focal point at the aperture thus forming an inverted image. Jaszczak and co-workers[4,5] originally proposed the extension of the cone-beam technology to SPECT imaging and later demonstrated that it offered an increase in efficiency of 2.5 times that of parallel-hole collimator systems with the same resolution.[6]

Various converging beam geometries have emerged for SPECT imaging of the brain. Two geometries were proposed by Jaszczak.[4,8] In one configuration, the focal point was asymmetrically located below the detector. In the second configuration, the focal point was symmetrically located relative to the face of the camera, but the camera was tilted so that it could come close to the head yet still clear the shoulders. Still another collimator configuration was proposed by Hawman and Hsieh[7] in which the collimator holes converge to two distinct lines which are orthogonal but at different distances from the face of the collimator. This astigmatic collimator was designed so that the head, which is more elliptical than circular, could fit better within the field of view.

In our application of heart imaging,[13] we have considered only a symmetric cone-beam geometry as shown in Fig. 1. The focal point is symmetrically located and the camera face remains parallel to the axis of rotation. The application of cone-beam collimation should give a significant increase in efficiency over that which is obtained with present cardiac SPECT imaging using parallel-hole collimators.

An important aspect of applying cone beam geometry to SPECT, in addition to the need for special reconstruction algorithms,[14-29] is the ability to measure precisely the geometrical parameters of the physical system consisting of col-

 0094-2405/90/020264-09$01.20

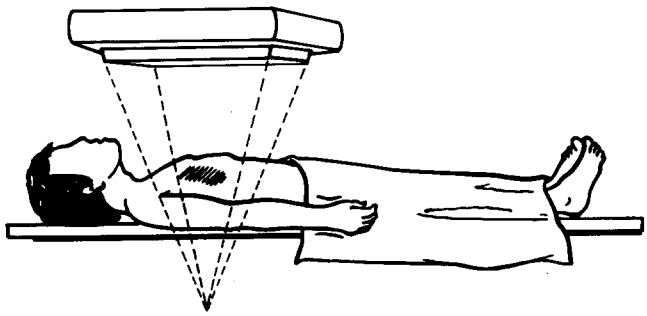

FIG. 1. Artist conception of cone-beam geometry for cardiac SPECT imaging.

limator and camera. The importance of this has previously been demonstrated for both parallel and fan-beam geometries to insure high-quality, artifact-free reconstructed images.[30–33] For parallel geometry, the perpendicular projection of the center of rotation onto the camera face is required and needs to be determined periodically in case there is any change in camera electronics or gantry mechanics. A point source or a line source is placed off the center of rotation and several complementary views 180° apart are obtained. The transverse coordinate of the projection of the center of rotation onto the image plane is determined by summing the transverse coordinate of the centroid of the projected point source in two complementary views and dividing by two. The average projection of the center of rotation is then determined by averaging the values obtained from all the complementary views.

Recently[33] we showed that the geometrical parameters for a fan-beam geometry could also be measured from projections of a point source. Here we extend this method to a symmetrical cone-beam geometry, but the methods are also applicable to various other cone-beam geometries. Equations are presented that relate the geometrical parameters to the centroid of the projections of a point source. As in the fan-beam case, the measured projections are not a linear function of the geometrical parameters; therefore, nonlinear techniques are required to estimate the parameter values. Results are presented where the method was used to estimate the geometrical parameters of a SPECT system with a cone-beam collimator. We show that the technique is also useful for evaluating the accuracy and precision of the manufactured collimator.

II. CONE-BEAM GEOMETRY FORMULATION

The parameters of the cone-beam geometry shown in Fig. 2 are the distance D from the focal point to the center of rotation (focus-to-center distance), focal length D' (the focus-to-detector distance), and the location (c_ξ, c_ζ) of the projection of the center of rotation onto the camera face. Notice that it is assumed that the center of rotation lies along the line of the perpendicular projection of the focal point. In previous work with fan-beam collimators,[33] a parameter was included to allow for any potential shift in the center of rotation off of the midline of the fan beam. However, it was found that the estimated value for the shift was very close to zero for a well-constructed collimator.[33] Also, computer simulations showed that the additional shift parameter complicated the problem because it is highly correlated with the projection coordinates of the center of rotation and can produce erroneous results for the estimated parameters if the initial estimates are not carefully selected. For these reasons, a shift parameter was not used in the cone-beam formulation.

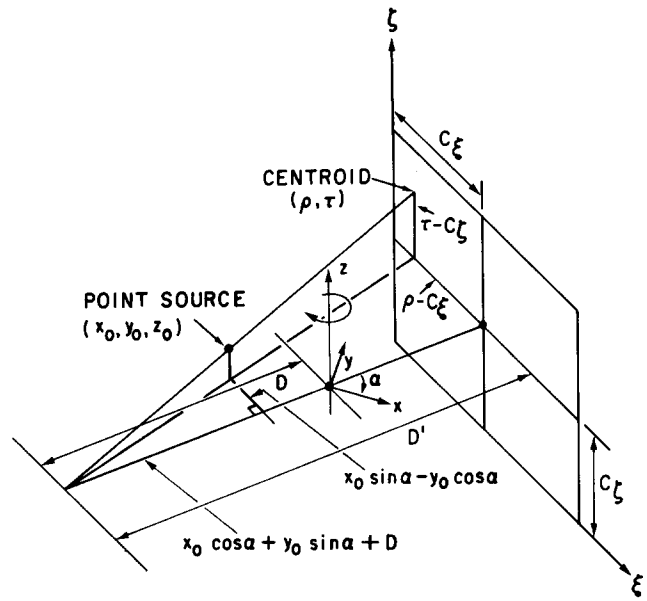

FIG. 2. The parameters $x_0, y_0, z_0, c_\xi, c_\zeta, D, D'$ of the cone-beam geometry are estimated by placing a point source at (x_0, y_0, z_0) and obtaining data for various projection angles α. Eqs. (8) and (9) give the functional relationship between these geometrical parameters and the centroid coordinates (ρ,τ).

The equation for the cone-beam projection operator can be derived using the expressions

$$(\xi - c_\xi)/D' = (x \sin\alpha - y \cos\alpha)/ (x \cos\alpha + y \sin\alpha + D) , \quad (1)$$

$$(\zeta - c_\zeta)/D' = z/(x \cos\alpha + y \sin\alpha + D) , \quad (2)$$

which are derived from the similar triangles shown in Fig. 2. These parametric equations describe a line of projection for the cone-beam geometry and relate the object coordinates (x, y, z) to the projection coordinates (α,ξ,ζ) where the coordinates ξ and ζ denote the corresponding distances from the edges of the measurable detector region and α is the projection angle. Using the expressions in Eqs. (1) and (2), one can write the cone-beam projection operator in terms of the product of two delta functions:

$$P(\alpha,\xi,\zeta) = \int_{-\infty}^{\infty}\int_{-\infty}^{\infty}\int_{-\infty}^{\infty} f(x,y,z)\delta[(\xi - c_\xi)(x\cos\alpha + y\sin\alpha + D)/D' - x\sin\alpha + y\cos\alpha] \times \delta[(\zeta - c_\zeta)(x\cos\alpha + y\sin\alpha + D)/D' - z]\, dx\, dy\, dz . \quad (3)$$

Mathematically, a point source

$$f(x,y,z) = \delta(x - x_0)\delta(y - y_0)\delta(z - z_0) , \quad (4)$$

located at (x_0, y_0, z_0) is used to develop a relationship between the parameters of the cone-beam geometry shown

in Fig. 2 and some measurable parameters; namely, the centroids of the projected point source. An expression for the projections of the point source is obtained by substituting Eq. (4) into Eq. (3) to give

$$R(\alpha,\xi,\zeta;\beta) = \delta[(\xi - c_\xi)(x_0\cos\alpha + y_0\sin\alpha + D)/D' - x_0\sin\alpha + y_0\cos\alpha] \times \delta[(\zeta - c_\zeta)(x_0\cos\alpha + y_0\sin\alpha + D)/D' - z_0], \quad (5)$$

where $\beta = (c_\xi, c_\zeta, D', D, x_0, y_0, z_0)$ is a vector with components which are the parameters of the cone-beam geometry plus the coordinates of the point source. For the angle α, the centroid of a projection is $[\rho(\alpha;\beta),\tau(\alpha;\beta)]$ defined by

$$\rho(\alpha;\beta) = \int_{-\infty}^{\infty}\int R(\alpha,\xi,\zeta;\beta)\,\xi\,d\xi\,d\zeta \Big/ \int_{-\infty}^{\infty}\int R(\alpha,\xi,\zeta;\beta)\,d\xi\,d\zeta, \quad (6)$$

$$\tau(\alpha;\beta) = \int_{-\infty}^{\infty}\int R(\alpha,\xi,\zeta;\beta)\,\zeta\,d\xi\,d\zeta \Big/ \int_{-\infty}^{\infty}\int R(\alpha,\xi,\zeta;\beta)\,d\xi\,d\zeta. \quad (7)$$

Substituting Eq. (5) into Eqs. (6) and (7) and integrating, we obtain the following expressions for the centroid coordinates in terms of the parameters for the cone-beam geometry:

$$\rho(\alpha;\beta) = D'(x_0\sin\alpha - y_0\cos\alpha)/(x_0\cos\alpha + y_0\sin\alpha + D) + c_\xi, \quad (8)$$

$$\tau(\alpha;\beta) = D'z_0/(x_0\cos\alpha + y_0\sin\alpha + D) + c_\zeta. \quad (9)$$

The geometrical parameters of a cone-beam imaging system are estimated by obtaining experimental measurements of a point source which is placed in the field of view of the scanner away from the center of rotation. Projections of the point source are collected and usually digitized into 64×64 or 128×128 matrices. By discretizing Eqs. (6) and (7), the centroids, $(\hat\rho_m,\hat\tau_m)$, $m = 1,\ldots,M$, are determined for each of the M projection matrices at angles α_m using:

$$\hat\rho_m = \sum_{k=1}^{N}\sum_{n=1}^{N}\xi_n\hat R(\alpha_m,\xi_n,\zeta_k) \Big/ \sum_{k=1}^{N}\sum_{n=1}^{N}\hat R(\alpha_m,\xi_n,\zeta_k), \quad (10)$$

$$\hat\tau_m = \sum_{k=1}^{N}\sum_{n=1}^{N}\zeta_k\hat R(\alpha_m,\xi_n,\zeta_k) \Big/ \sum_{k=1}^{N}\sum_{n=1}^{N}\hat R(\alpha_m,\xi_n,\zeta_k), \quad (11)$$

where $\hat R(\alpha_m,\xi_n,\zeta_k)$, $n = 1,\ldots,N$, $k = 1,\ldots,N$, are the sampled intensities in the projection matrices.

The parameters of the cone-beam geometry are estimated by minimizing the chi-square (χ^2) function

$$\chi^2(\beta) = \sum_m \{[\hat\rho_m - \rho(\alpha_m;\beta)]^2/\sigma^2_{\rho m} + [\hat\tau_m - \tau(\alpha_m;\beta)]^2/\sigma^2_{\tau m}\}, \quad (12)$$

where $\rho(\alpha_m;\beta)$ and $\tau(\alpha_m;\beta)$ are given in Eqs. (8) and (9); and $(\hat\rho_m,\hat\tau_m)$ are the centroids calculated in Eqs. (10) and (11). Assuming Poisson statistics, the variances $\sigma^2_{\rho m}$ and $\sigma^2_{\tau m}$ are determined from Eqs. (10) and (11) using propagation of errors to give

$$\sigma^2_{\rho m} = \left\{\left[\sum_k\sum_n \xi_n^2\hat R(\alpha_m,\xi_n,\zeta_k)\right]\left[\sum_k\sum_n\hat R(\alpha_m,\xi_n,\zeta_k)\right]^2 - \left[\sum_k\sum_n\xi_n\hat R(\alpha_m,\xi_n,\zeta_k)\right]^2\left[\sum_k\sum_n\hat R(\alpha_m,\xi_n,\zeta_k)\right]\right\} \times\left[\sum_k\sum_n\hat R(\alpha_m,\xi_n,\zeta_k)\right]^{-4}, \quad (13)$$

$$\sigma^2_{\tau m} = \left\{\left[\sum_k\sum_n \zeta_k^2\hat R(\alpha_m,\xi_n,\zeta_k)\right]\left[\sum_k\sum_n\hat R(\alpha_m,\xi_n,\zeta_k)\right]^2 - \left[\sum_k\sum_n\zeta_k\hat R(\alpha_m,\xi_n,\zeta_k)\right]^2\left[\sum_k\sum_n\hat R(\alpha_m,\xi_n,\zeta_k)\right]\right\} \times\left[\sum_k\sum_n\hat R(\alpha_m,\xi_n,\zeta_k)\right]^{-4}. \quad (14)$$

One can show that the expressions in Eqs. (13) and (14) are approximately equal to the variance of the projected point source distribution divided by the number of samples.

III. ESTIMATION ALGORITHM

The process of minimizing Eq. (12) to determine estimates of the cone-beam geometry is a nonlinear estimation problem since the functions $\rho(\alpha;\beta)$ and $\tau(\alpha;\beta)$ in Eqs. (8) and (9) are nonlinear in the vector variable β. The χ^2 function in Eq. (12) is minimized by using an iterative algorithm. At the $i+1$th iteration, the estimate

$$\beta^{i+1} = \beta^i + \delta, \quad (15)$$

is obtained by adding to the estimate β^i at the ith iteration, a correction vector δ. The correction δ is determined by solving the following system of equations[34]:

$$(B + \lambda I)\delta = E, \quad (16)$$

where I denotes the identity matrix. The elements of the matrices B and E are given by

$$B = [b_{ij}]^{7\times7} = \left[\sum_{m=1}^{M}\frac{1}{\sigma^2_{\rho m}}\frac{\partial\rho(\alpha_m;\beta)}{\partial\beta_i}\frac{\partial\rho(\alpha_m;\beta)}{\partial\beta_j} + \sum_{m=1}^{M}\frac{1}{\sigma^2_{\tau m}}\frac{\partial\tau(\alpha_m;\beta)}{\partial\beta_i}\frac{\partial\tau(\alpha_m;\beta)}{\partial\beta_j}\right]^{7\times7}, \quad (17)$$

$$E = [e_i]^{1\times 7} = \left[\sum_{m=1}^{M} \frac{\partial \rho(\alpha_m;\beta)}{\partial \beta_i} [\hat{\rho}_m - \rho(\alpha_m;\beta)]/\sigma^2_{\rho m} + \sum_{m=1}^{M} \frac{\partial \tau(\alpha_m;\beta)}{\partial \beta_i} [\hat{\tau}_m - \tau(\alpha_m;\beta)]/\sigma^2_{\tau m} \right]^{1\times 7}, \quad (18)$$

where $(\beta_1,\ldots,\beta_7) = (c_\xi, c_\zeta, D', D, x_0, y_0, z_0)$. The value of λ is determined so that the correction vector δ is the optimum choice between a Taylor series correction vector and a gradient vector.

To obtain the partial derivatives in Eqs. (17) and (18), we set

$$g = D'(x_0 \sin\alpha - y_0 \cos\alpha) \quad (19)$$

and

$$h = x_0 \cos\alpha + y_0 \sin\alpha + D, \quad (20)$$

so that we might simplify Eqs. (8) and (9):

$$\rho(\alpha;\beta) = g/h + c_\xi, \quad (21)$$

$$\tau(\alpha;\beta) = D' z_0/h + c_\zeta. \quad (22)$$

Then it is possible to derive the partial derivatives of $\rho(\alpha;\beta)$ which are given by

$$\frac{\partial \rho}{\partial \beta_1} = \frac{\partial \rho}{\partial c_\xi} = 1, \quad (23)$$

$$\frac{\partial \rho}{\partial \beta_2} = \frac{\partial \rho}{\partial c_\zeta} = 0, \quad (24)$$

$$\frac{\partial \rho}{\partial \beta_3} = \frac{\partial \rho}{\partial D'} = g/(hD'), \quad (25)$$

$$\frac{\partial \rho}{\partial \beta_4} = \frac{\partial \rho}{\partial D} = -g/h^2, \quad (26)$$

$$\frac{\partial \rho}{\partial \beta_5} = \frac{\partial \rho}{\partial x_0} = [D'h \sin\alpha - g\cos\alpha]/h^2, \quad (27)$$

$$\frac{\partial \rho}{\partial \beta_6} = \frac{\partial \rho}{\partial y_0} = [-D'h\cos\alpha - g\sin\alpha]/h^2, \quad (28)$$

$$\frac{\partial \rho}{\partial \beta_7} = \frac{\partial \rho}{\partial z_0} = 0; \quad (29)$$

and the partial derivatives of $\tau(\alpha;\beta)$ which are given by

$$\frac{\partial \tau}{\partial \beta_1} = \frac{\partial \tau}{\partial c_\xi} = 0, \quad (30)$$

$$\frac{\partial \tau}{\partial \beta_2} = \frac{\partial \tau}{\partial c_\zeta} = 1, \quad (31)$$

$$\frac{\partial \tau}{\partial \beta_3} = \frac{\partial \tau}{\partial D'} = z_0/h, \quad (32)$$

$$\frac{\partial \tau}{\partial \beta_4} = \frac{\partial \tau}{\partial D} = -D' z_0/h^2, \quad (33)$$

$$\frac{\partial \tau}{\partial \beta_5} = \frac{\partial \tau}{\partial x_0} = -D' z_0 \cos\alpha/h^2, \quad (34)$$

$$\frac{\partial \tau}{\partial \beta_6} = \frac{\partial \tau}{\partial y_0} = -D' z_0 \sin\alpha/h^2, \quad (35)$$

$$\frac{\partial \tau}{\partial \beta_7} = \frac{\partial \tau}{\partial z_0} = D'/h. \quad (36)$$

The implementation of the Marquardt algorithm is outlined in our previous paper.[33] The algorithm selects λ to ensure that the optimum choice for δ is taken. An especially nice feature of the algorithm is that the direction and step size are determined simultaneously. Starting with initial estimates, new values of the geometrical parameters are determined from Eq. (15). The new estimates in the iterative algorithm sequentially approach a minimum solution to the χ^2 function in Eq. (12). At each iteration, the measured centroid of the projected point source is compared with the expression in Eqs. (8) and (9). Thus, the algorithm is effectively evaluating those parameters which make Eqs. (8) and (9) come nearest the measured centroid of the projected point source to obtain an optimum fit to the data.

The statistical errors in the estimated parameters are given by the covariance matrix[35]

$$\Phi = B^{-1}, \quad (37)$$

where the matrix B is evaluated substituting the estimated parameters into Eq. (17). The diagonal elements of the covariance matrix are the variances for the estimated parameters. The off-diagonal elements are the covariances which are a measure of the degree of correlation between the geometrical parameters.

For parameters that are highly correlated, the choice of the initial estimates becomes more important in terms of obtaining realistic solutions. It can happen, if the initial estimates are not near the correct values, the parameter estimates may converge to a local minimum with unrealistic results and still give a good fit to the data. Also, if these estimated parameter values are incorporated into the reconstruction algorithm, the reconstruction results will probably not show any image distortions. However, this is not very appealing if one wants to know a parameter exactly, such as one would in using the estimated collimator focal length to compare the manufactured accuracy with the designed specifications of the collimator. Therefore, it is suggested that the initial estimates be chosen carefully, and the degree to which this is important depends upon the parameter.

IV. EXPERIMENTAL RESULTS

A study was performed to evaluate the technique for estimating the parameters of a converging collimator (GE low-energy converging collimator, H2503AD, GE Medical Systems, Milwaukee, WI) for which the geometry is shown in Fig. 3. A point source of ^{99m}Tc was placed at four separate positions in four separate studies. For each point source location, the camera (GE 400 AC/T, GE Medical Systems, Milwaukee, WI) was rotated about its center of rotation to obtain a set of 128 projections over 360°. Each projection data set illustrated in Fig. 4 was digitized into a 64×64 array representing 6.4-mm pixels in the image plane.

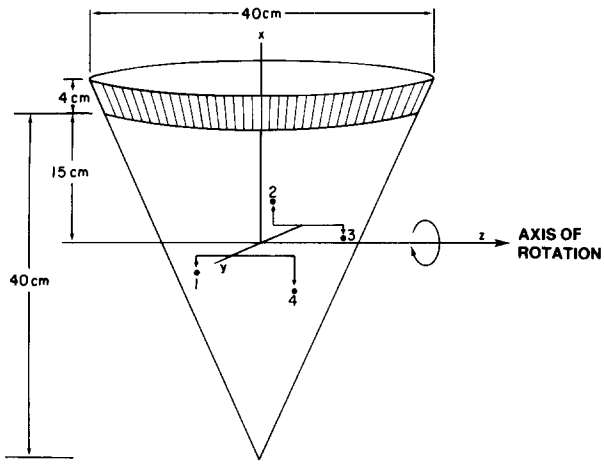

FIG. 3. The experimental setup showing the location of the point sources for each of the four studies and the dimensions of the cone-beam geometry.

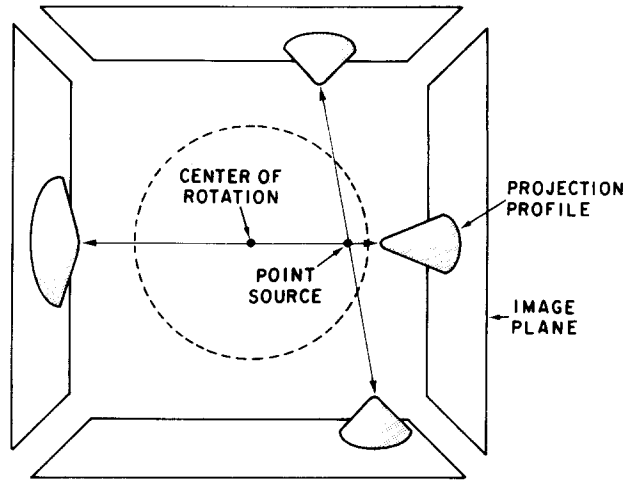

FIG. 4. Sketch showing the projections of the point source onto the two-dimensional detector. Using Eqs. (10) and (11) the centroids $(\hat{\rho},\hat{\tau})$ of these two-dimensional projections were calculated. Notice that profiles change as a function of the distance the camera is away from the point source.

After the data were acquired, the centroid coordinates for each projection were determined using Eqs. (10) and (11) and the measurement errors for the centroid calculations were determined using Eqs. (13) and (14). Table I lists for every other angle sampled over 360°, the coordinates and the errors for the projected centroids of the point source labeled 3 in Fig. 3. The data show small statistical errors and are representative of data from the other three point source locations. In comparing these errors with those calculated from a one-dimensional data set used to estimate the parameters for

TABLE I. Centroids [Eqs. (10) and (11)] and errors [Eqs. (13) and (14)] are calculated from cone beam projection data for the point source positioned at location 3 in Fig. 3.

		Centroid		Errors				Centroid		Errors	
Frame	Angle (Degs)	$\hat{\rho}$ (cm)	$\hat{\tau}$ (cm)	σ_ρ (cm)	σ_τ (cm)	Frame	Angle (Degs)	$\hat{\rho}$ (cm)	$\hat{\tau}$ (cm)	σ_ρ (cm)	σ_τ (cm)
1	0	27.5972	29.4439	0.0095	0.0093	65	180.0	14.7433	29.2305	0.0091	0.0102
3	5.6	27.6134	29.6028	0.0086	0.0091	67	185.6	14.9524	29.0984	0.0094	0.0106
5	11.2	27.5216	29.7391	0.0085	0.0091	69	191.2	15.2223	28.9960	0.0094	0.0103
7	16.8	27.3440	29.8599	0.0085	0.0092	71	196.8	15.5141	28.9188	0.0092	0.0100
9	22.5	27.1045	30.0194	0.0085	0.0082	73	202.5	15.8701	28.8032	0.0092	0.0102
11	28.1	26.7954	30.1145	0.0086	0.0093	75	208.1	16.2538	28.7082	0.0092	0.0106
13	33.8	26.3783	30.2639	0.0085	0.0094	77	213.8	16.6661	28.6421	0.0093	0.0108
15	39.4	25.9226	30.4012	0.0081	0.0092	79	219.4	17.0868	28.5946	0.0088	0.0107
17	45.0	25.3945	30.5528	0.0078	0.0090	81	225.0	17.5538	28.5630	0.0087	0.0104
19	50.6	24.8023	30.6676	0.0080	0.0093	83	230.6	18.0621	28.5541	0.0091	0.0106
21	56.2	24.1616	30.8266	0.0077	0.0089	85	236.2	18.5922	28.5533	0.0088	0.0107
23	61.8	23.4716	30.9453	0.0076	0.0089	87	241.8	19.1213	28.5372	0.0092	0.0111
25	67.5	22.7611	31.0297	0.0077	0.0093	89	247.5	19.6497	28.5219	0.0088	0.0106
27	73.1	22.0165	31.1184	0.0075	0.0090	91	253.1	20.2411	28.4766	0.0094	0.0111
29	78.8	21.1759	31.1580	0.0076	0.0092	93	258.8	20.8124	28.4394	0.0090	0.0109
31	84.4	20.3448	31.2244	0.0078	0.0090	95	264.4	21.4098	28.3871	0.0095	0.0114
33	90.0	19.4993	31.2982	0.0078	0.0090	97	270.0	21.9946	28.3620	0.0094	0.0112
35	95.6	18.6834	31.3621	0.0077	0.0089	99	275.6	22.6005	28.3599	0.0098	0.0113
37	101.2	17.8994	31.3576	0.0075	0.0091	101	281.2	23.1638	28.3595	0.0103	0.0117
39	106.8	17.1919	31.3016	0.0072	0.0091	103	286.8	23.6714	28.3370	0.0105	0.0019
41	112.5	16.6273	31.1913	0.0073	0.0091	105	292.5	24.1749	28.3546	0.0104	0.0121
43	118.1	16.1057	31.0711	0.0072	0.0090	107	298.1	24.6697	28.3807	0.0103	0.0116
45	123.8	15.6892	30.8984	0.0074	0.0092	109	303.8	25.1389	28.4285	0.0105	0.0113
47	129.4	15.3270	30.7228	0.0072	0.0091	111	309.4	25.5589	28.4873	0.0107	0.0118
49	135.0	14.0429	30.5432	0.0076	0.0089	113	315.0	25.9156	28.5345	0.0110	0.0115
51	140.6	14.8179	30.3442	0.0077	0.0093	115	320.6	26.3059	28.6166	0.0108	0.0115
53	146.2	14.6872	30.1673	0.0083	0.0094	117	326.2	26.6341	28.7213	0.0106	0.0111
55	151.8	14.5483	30.0030	0.0078	0.0092	119	331.8	26.9009	28.8259	0.0105	0.0107
57	157.5	14.5038	29.8450	0.0085	0.0093	121	337.5	27.1502	28.9522	0.0104	0.0107
59	163.1	14.4773	29.6706	0.0085	0.0095	123	343.1	27.3512	29.0926	0.0103	0.0103
61	168.8	14.5087	29.5047	0.0089	0.0100	125	348.8	27.4973	29.2111	0.0101	0.0101
63	174.4	14.6118	29.3525	0.0093	0.0130	127	354.4	27.5946	29.3563	0.0095	0.0099

a fan-beam geometry,[33] the errors in Table I are an order of magnitude smaller due primarily to the larger sample size of the two-dimensional data set. In addition, the precision in the centroid measurements, given in terms of the statistical errors, is less than a millimeter; whereas, the measurement accuracy is significantly larger since the sampling pixel size of 6.4 mm is fairly coarse. Therefore, the precision given in Table I should only be interpreted in terms of the outcome of repeated measurements; that is, if the measurement is repeated, the result would be (barring any systematic errors) within the same value $\pm$ the quoted error at a confidence level of 67%.

The initial estimates were chosen carefully to be as close to the actual value as possible to avoid settling on any local minimum that would give unrealistic solutions. The initial values that were assigned to each of the geometrical parameters, c_ξ, c_ζ, D', D, x_0, y_0, and z_0 are given in Table II for each point source location. The coordinates (x_0, y_0, z_0) of each point source were initially set to zero. The projection of the focal point and the center of rotation onto the detector is usually near the center of the crystal, so values of $c_\xi = 20$ cm, $c_\zeta = 20$ cm were chosen as the initial estimate. The collimator was built to a designed specification for the focal length of ~40 cm. Thus, a value of 45 cm was chosen as an initial estimate for D' in order to include the focus-to-collimator distance plus the length of the collimator holes, the gap between the collimator and crystal, and any potential crystal penetration. The focus-to-center distance D was chosen to be fixed at 25 cm, which is the designed focus-to-collimator distance of 40 cm shown in Fig. 3, minus the distance of 15 cm, which was the distance the center of rotation was placed from the face of the collimator.

After the initial solutions were set, the geometrical parameters were systematically and iteratively varied using the Marquardt algorithm[33,34] to minimize the χ^2 function in Eq. (12). It was found useful to vary only certain of the parameters at first to increase their precision before varying others. The results in Table II first varied x_0, y_0, and z_0 only, holding the other geometrical parameters constant. The second pass varied c_ξ and c_ζ only, the third pass varied D', and the last pass allowed all parameters except for D to vary.

In general, the fitting technique most accurately determines the projected center of rotation coordinates (c_ξ, c_ζ). Various initial solutions were tested and in all cases, c_ξ con-

TABLE II. Estimates for the geometrical parameters were obtained for each point source placed at four separate locations shown in Fig. 3. In each pass, those variables indicated with an asterisk are held constant and the other variables are allowed to vary using the Marquardt algorithm to give a best estimate of the parameters. The errors for each estimate are given in parentheses and all values are in units of cm.

Pass	c_ξ	c_ζ	D'	D	x_0	y_0	z_0	χ^2
Initial value	20	20	45	25	0	0	0	
				POINT SOURCE LOCATION 1				
1	20*	20*	45*	25*	−0.3013 (±0.0005)	3.5905 (±0.0005)	−2.5360 (±0.0004)	2046721
2	20.9640 (±0.0007)	20.0031 (±0.0008)	45*	25*	−0.3013*	3.5905*	−2.5360*	164252
3	20.9640*	20.0031*	45.2967 (±0.0050)	25*	−0.3013*	3.5905*	−2.5360*	160728
4	21.0026 (±0.0007)	20.1737 (±0.0008)	45.0606 (±0.0041)	25*	−0.1686 (±0.0005)	3.6433 (±0.0002)	−2.6232 (±0.0001)	87865
				POINT SOURCE LOCATION 2				
1	20*	20*	45*	25*	1.5858 (±0.0005)	−3.5678 (±0.0006)	−1.7674 (±0.0004)	1897524
2	20.9792 (±0.0007)	20.0025 (±0.0007)	45*	25*	1.5858*	−3.5678*	−1.7674*	130225
3	20.9792*	20.0025*	45.2153 (±0.0057)	25*	1.5858*	−3.5678*	−1.7674*	128761
4	21.0310 (±0.0007)	20.0166 (±0.0007)	41.9731 (±0.0048)	25*	1.5470 (±0.0006)	−3.9119 (±0.0003)	−1.8952 (±0.0002)	33645
				POINT SOURCE LOCATION 3				
1	20*	20*	45*	25*	−0.4952 (±0.0006)	−3.5910 (±0.0006)	5.2696 (±0.0005)	1629821
2	20.9324 (±0.0008)	19.9962 (±0.0009)	45*	25*	−0.4952*	−3.5910*	5.2696*	148514
3	20.9419*	19.9754*	45.1558 (±0.0036)	25*	−0.4952*	−3.5910*	5.2696*	146594
4	20.9701 (±0.0014)	21.7712 (±0.0016)	35.9526 (±0.0060)	25*	−0.7844 (±0.0013)	−4.5040 (±0.0013)	5.3371 (±0.0011)	68370
				POINT SOURCE LOCATION 4				
1	20*	20*	45*	25*	−3.5726 (±0.0006)	3.2898 (±0.0006)	5.1935 (±0.0005)	1293960
2	20.9377 (±0.0009)	19.9972 (±0.0010)	45*	25*	−3.5726*	3.2898*	5.1935*	146176
3	20.9377*	19.9972*	45.0829 (±0.0052)	25*	−3.5726*	3.2898*	5.1935*	145657
4	20.9896 (±0.0009)	21.4699 (±0.0010)	37.3677 (±0.0027)	25*	−4.1566 (±0.0006)	4.0719 (±0.0003)	5.2397 (±0.0002)	60915

verged very closely to 21 cm. The estimates for the centroid coordinate c_ζ seemed to vary with the position of the point source more than that of c_ξ. In the four studies, the largest variations in the estimates were obtained for the focal length D' which ranged between 45.06 and 35.95 cm. We also found if D was a variable, that for different initial values assigned to the parameters, the algorithm converged to different estimates for D and the point source coordinates (x_0, y_0, z_0); whereas, the other parameters would always converge to nearly the same solution. This is not too surprising considering that the point source coordinates and the distance from the focal point to the center of rotation are highly correlated. Therefore, D was chosen to be fixed at 25 cm for all the results presented in Table II.

An independent study was performed where point sources were positioned at different locations away from the crystal and at different locations parallel to the plane of the collimator. The focal length that was calculated for different positions parallel to the face of the collimator correlated well with the estimated values using our fitting technique, and indicated that the focal length did indeed vary across the face of the collimator. The cause of the focal length variation is most likely the result of deviations in the collimator hole angulation from the designed specifications and is not unlike experiences with parallel-hole collimators.[36,37]

An example of the fit (ρ,τ) for the calculated centroid coordinates $\hat{\rho}$ and $\hat{\tau}$ as a function of angle is shown in Fig. 5 for the data obtained from point source location 3. The differences between the measured data and the fit as a function of angle for each of the four studies is shown in Fig. 6. Visually, one can see that the best fit is obtained in Fig. 6(b) for point source location 2, and this is substantiated by its lowest χ^2 value in Table II. In all the studies, the best fits seem to be obtained for the centroid coordinate ρ perpendicular to the axis of rotation.

The large χ^2 values in Table II are due to the division in Eq. (12) of the square of relatively large differences between the fit and the measured data (absolute value <0.4 cm) by very small measurement errors (<0.0001 cm). These relatively large differences appear to be due to systematic errors in the data. If one looks closely at the measured curves in Fig. 5, the plot for the measured coordinate $\hat{\tau}$ does not appear to be smoothly varying but has small bends in the curve. From the different estimated focal lengths obtained for different point source locations, one would infer that these systematic errors are due to variations in the focal length caused by perturbations in the hole angulation across the collimator.

Previous work with parallel collimators indicate that variations in the coordinate $\hat{\tau}$ parallel to the axis of rotation is a good measure of the variation in the angulation of the collimator holes.[37] If we consider the projection data that are obtained as the camera is rotated 360° around the point source, during the rotation, rays from the source pass through a series of holes across the face of the collimator. For parallel-hole collimators, the series of holes are orthogonal to the axis of rotation; thus, the plot of the calculated centroid $\hat{\tau}$ should be a straight horizontal line. In contrast, for converging collimators the series of holes are not orthogonal to the axis of rotation and the plot should be a slowly varying curve. Visual interpretation of the curved path is useful to show systematic deviations which are not random, thereby, providing a good indication of the deviations in the hole angulation for those holes traversed by the point source during the rotation.

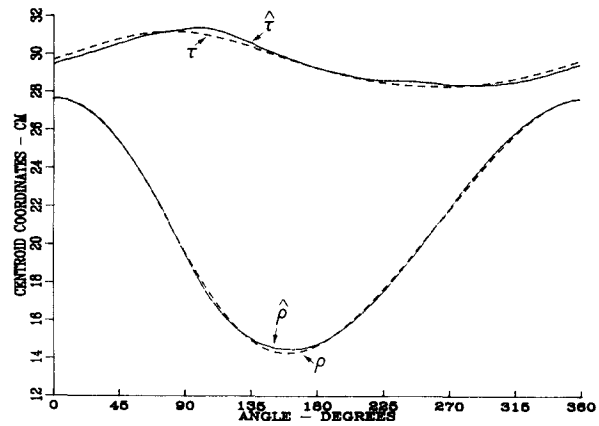

FIG. 5. Plots of the estimated (ρ,τ) and the measured $(\hat{\rho},\hat{\tau})$ centroid coordinates for the data in Table I (point source location 3).

V. DISCUSSION AND CONCLUSION

We have presented a method that is able to measure the parameters of a cone-beam detector system using a nonlinear estimation technique that estimates the geometrical parameters from data which are projection measurements of a point source. The method involves calculating over 360° the coordinates of the centroids of the projected point source and then using the Marquardt algorithm to fit the measured centroid coordinates to analytical expressions of the coordinates in terms of the geometrical parameters. The method was also found to be useful in evaluating the accuracy of the collimator construction by measuring variations in the estimated focal length as point sources are placed at different positions in the field of view. The focal length variations are due to deviations in the constructed collimator hole angulation from the designed angulation which is intended to focus each hole to a common focal point.

Collimator manufacturers have indicated that the large focal length variations observed in the collimator which we tested is not too surprising for collimators manufactured several years ago. They claim that the manufacturing process has improved significantly and that the new collimators are constructed with a focal length variation guaranteed to be within a tolerance of 2 mm. However, the variability in the collimator hole angulation and the center of rotation across the crystal should be measured and should preclude acceptance of any newly manufactured collimator to be used by a SPECT system as it has recently been recommended for parallel-hole collimators.[37,38] Since cone-beam tomography is used to estimate geometrical parameters, the estimated focal length is an average for a series of collimator holes; thus, it is also recommended that the focal lengths be verified directly using a device such as a three-dimensional rectangular tray holder that is able to support a series of point sources at several distances away from the collimator.[36,37]

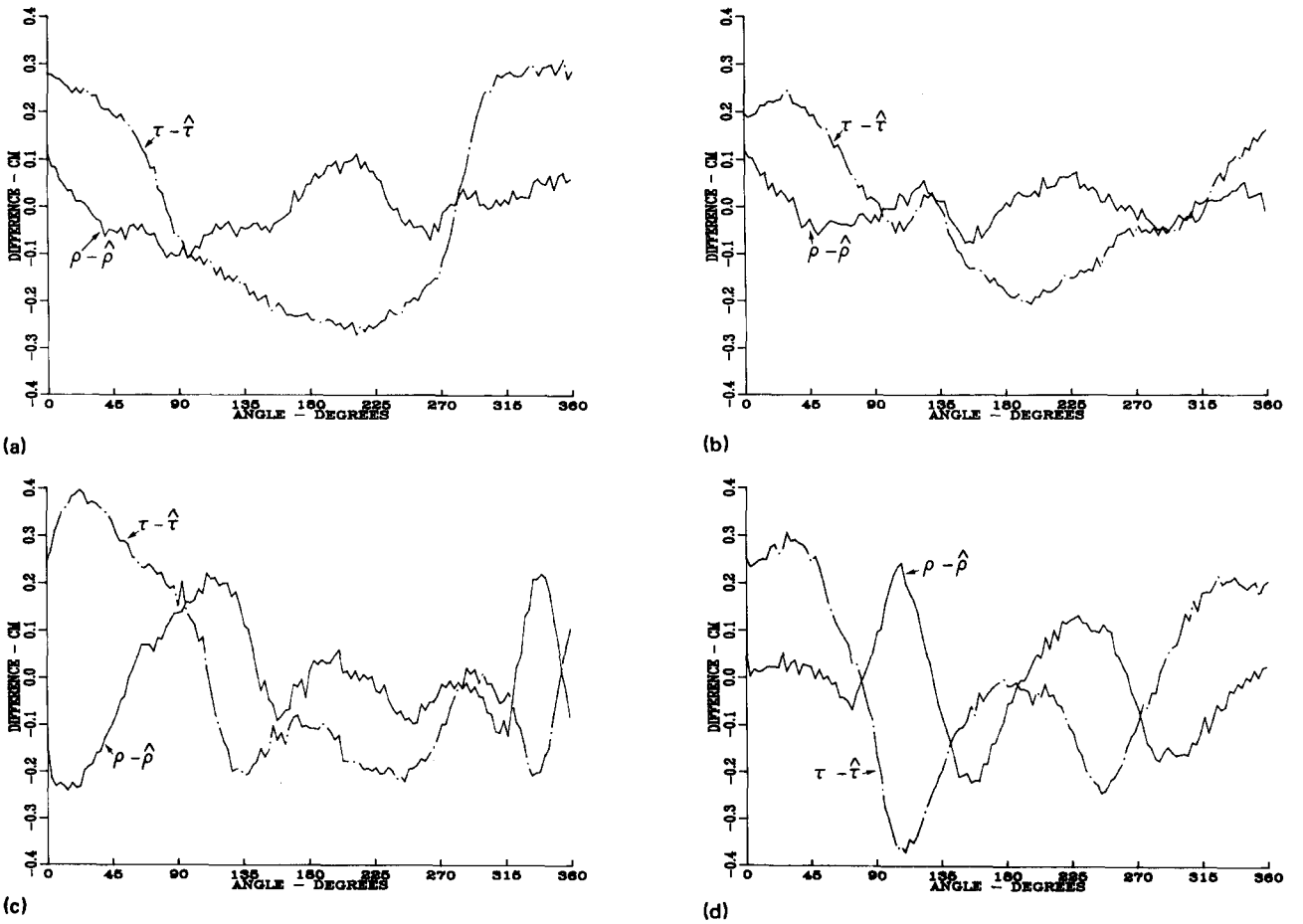

FIG. 6. Plots of the difference between the estimated and measured centroid coordinates for the data from the point source (a) at location 1, (b) at location 2, (c) at location 3, and (d) at location 4 in Fig. 3.

The estimation technique can provide several parameters; but, estimates for the focal length D' and the projection of the center of rotation onto the detector (c_ξ, c_ζ) completely specifies the reconstruction geometry and is all that is required to reconstruct clinical cone-beam data. In filtered backprojection[22] and iterative reconstruction algorithms,[29] the estimated focal length is expressed in units of the sampling bin width at the detector; this is equivalent to transforming the reconstruction problem into one where the detector is located at the center of rotation.[39] The choice of the pixel width (in units of projection bin width) of the reconstructed image is arbitrary and is set by the user depending upon the size of the desired reconstructed pixel (larger pixels less counts per pixel, smaller pixels more counts per pixel). The coordinates for (c_ξ, c_ζ), also expressed in units of projection bin width, are used to position the projection array relative to the center of rotation of the reconstructed coordinate system, so that at any desired projection angle the image pixels can be correctly related to the projection bin into which they project.

Knowledge of the distance D between the focal point and the center of rotation becomes important when the reconstructed pixel size is required for quantitation purposes. In our technique, D was fixed because we found that D was highly correlated with the point source coordinates and accurate values for D where difficult to obtain. In a quantitative clinical study, it may be advisable to determine the distance D using more accurate methods such as using a laser stereotaxic system. It can be shown that specifying D is equivalent to imposing a scaling of the pixel width and would either minify or magnify the image. In this way, the reconstruction problem is somewhat arbitrary as to where one wants to choose the focus-to-center distance D. It also implies that the important thing in relating the reconstructed pixels to the corresponding sample bin is the angle of arc subtended by a sampling bin. Therefore, incorrectly specifying D does not result in reconstruction artifacts, but is important in obtaining quantitative measurements.

The estimated parameters obtained by tomography are an average for a series of collimator holes. Reconstruction artifacts can result if there are large variations in the actual focal length and center of rotation across the camera field of view. In our previous experience with fan-beam collimators, the focal length can vary significantly (more than 10 cm) and reconstruction artifacts are not observed.[33] However, one should keep in mind that those observations were made based upon results obtained using a long focal length collimator (72 cm) and the tolerance will more likely be less for shorter focal lengths. However, the critical parameter is c_ξ. Variations in this can cause significant errors in the reconstructed image as it does for parallel and fan-beam geometries.[30–33]

The method presented in this paper should be useful to evaluate initially the quality of the converging collimator, in

particular, the uniformity of the focal length. It is necessary to only determine the collimator focal length once since the focal length is fixed by the collimator and remains unchanged. However, the estimation technique should periodically be used to recalculate, in case of any electronic changes, the coordinates of the projection of the center of rotation, just as is done presently with parallel geometry.[38] The tolerances for these parameters still need to be determined in terms of the necessary requirements for good image quality. The question of how correlations between parameters effect the estimation results, especially with the potential of including other parameters such as center of rotation shifts, need to be investigated for the potential of using the estimation technique for a variety of quality control testing procedures.

ACKNOWLEDGMENTS

The research work presented in this manuscript was partially supported by Public Health Service Grants, Nos. R01 CA 39463 and R01 HL 39792, and The Whitaker Foundation.

[1]R. J. Jaszczak, L.-T. Chang, and P. H. Murphy, "Single photon emission computed tomography using multi-slice fan beam collimators," IEEE Trans. Nucl. Sci. **26**, 610–618 (1979).

[2]C. B. Lim, L.-T. Chang, and R. J. Jaszczak, "Performance analysis of three camera configurations for single photon emission computed tomography," IEEE Trans. Nucl. Sci. **27**, 559–568 (1980).

[3]B. M. W. Tsui, G. T. Gullberg, E. R. Edgerton, D. R. Gilland, J. R. Perry, W. H. McCartney, "Design and clinical utility of a fan beam collimator for SPECT imaging of the head," J. Nucl. Med. **27**, 810–819 (1986).

[4]R. J. Jaszczak, C. E. Floyd, Jr., C. C. Harris, and R. E. Coleman, "Cone beam collimation for SPECT: Improved data acquisition geometry," Radiology **157**(P), 61 (1985).

[5]C. E. Floyd, Jr., R. J. Jaszczak, S. H. Manglos, K. L. Greer, C. C. Harris, and R. E. Coleman, "Cone beam reconstruction for SPECT using inverse Monte Carlo," Radiology **157**(P), 320 (1985).

[6]R. J. Jaszczak, C. E. Floyd, Jr., S. H. Manglos, K. L. Greer, and R. E. Coleman, "Cone beam collimation for single photon emission computed tomography: Analysis, simulation, and image reconstruction using filtered backprojection," Med. Phys. **13**, 484–489 (1986).

[7]E. G. Hawman and J. Hsieh, "An astigmatic collimator for high sensitivity SPECT of the brain," J. Nucl. Med. **27**, 930 (1986).

[8]R. J. Jaszczak, K. L. Greer, and R. E. Coleman, "SPECT using a specially designed cone beam collimator," J. Nucl. Med. **29**, 1398–1405 (1988).

[9]S. Rudin, P. A. Bardfeld, and H. Hart, "Use of magnifying multihole collimators in the gamma-ray camera system," J. Nucl. Med. **12**, 831–834 (1971).

[10]J. E. Dowdey and F. J. Bonte, "Principles of scintillation camera image magnification with multichannel convergent collimators," Radiology **104**, 89–96 (1972).

[11]R. A. Moyer, "A low-energy multihole converging collimator compared with a pinhole collimator," J. Nucl. Med. **15**, 59–64 (1974).

[12]B. M. W. Tsui and G. T. Gullberg, "The geometric transfer function for cone and fan beam collimators," Phy. Med. Biol. **35**, 81–93 (1990).

[13]G. T. Gullberg, G. L. Zeng, P. E. Christian, B. M. W. Tsui, and H. T. Morgan, "Single photon emission computed tomography of the heart using cone beam geometry and noncircular detector rotation," in *Information Processing in Medical Imaging*, XIth IPMI International Conference, Berkeley, CA, 1989 (in press).

[14]M. D. Altschuler, G. T. Herman, and A. Lent, "Fully three-dimensional image reconstruction from cone-beam sources," in *Proceedings of the Conference on Pattern Recognition and Image Processing* (IEEE Computer Society, Long Beach, California, 1978), pp. 194–199.

[15]O. Nalcioglu and Z. H. Cho, "Reconstruction of 3-D objects from cone beam projections," Proc. IEEE **66**, 1584–1585 (1978).

[16]G. N. Minerbo, "Convolutional reconstruction from cone-beam projection data," IEEE Trans. Nucl. Sci. **26**, 2682–2684 (1979).

[17]G. Kowalski, "Multislice reconstruction from twin-cone beam scanning," IEEE Trans. Nucl. Sci. **26**, 2895–2903 (1979).

[18]G. N. Minerbo, "Maximum entropy reconstruction from cone-beam projection data," Comput. Biol. Med. **9**, 29–37 (1979).

[19]R. V. Denton, B. Friedlander, and A. J. Rockmore, "Direct three-dimensional image reconstruction from divergent rays," IEEE Trans. Nucl. Sci. **26**, 4695–4703 (1979).

[20]H. K. Tuy, "An inversion formula for cone-beam reconstruction," SIAM J. Appl. Math. **43**, 546–552 (1983).

[21]B. D. Smith, "Cone beam convolution formula," Comp. Biol. Med. **13**, 81–87 (1983).

[22]L. A. Feldkamp, L. C. Davis, and J. W. Kress, "Practical cone-beam algorithm," J. Opt. Soc. Am. A **1**, 612–619 (1984).

[23]F. C. Peyrin, "The generalized back projection theorem for cone beam reconstruction," IEEE Trans. Nucl. Sci. **32**, 1512–1519 (1985).

[24]D. V. Finch, "Cone beam reconstruction with sources on a curve," SIAM J. Appl. Math. **45**, 665–673 (1985).

[25]C. E. Floyd, Jr., R. J. Jaszczak, K. L. Greer, and R. E. Coleman, "Cone beam collimation for SPECT: simulation and reconstruction," IEEE Trans. Nucl. Sci. **33**, 511–514 (1986).

[26]S. Webb, J. Sutcliffe, L. Burkinshaw, and A. Horsman, "Tomographic reconstruction from experimentally obtained cone-beam projections," IEEE Trans. Med. Imag. **6**, 67–73 (1987).

[27]S. H. Manglos, R. J. Jaszczak, C. E. Floyd, Jr., K. L. Greer, and R. E. Coleman, "A practical attenuation compensation method for cone beam SPECT," IEEE Trans. Nucl. Sci. **34**, 294–298 (1987).

[28]S. H. Manglos, R. J. Jaszczak, and J. G. McAfee, "Maximum likelihood reconstruction for cone beam SPECT with camera tilt," IEEE Trans. Nucl. Sci. **36**, 1117–1121 (1989).

[29]G. T. Gullberg, G. L. Zeng, B. M. W. Tsui, J. T. Hagius, "Iterative reconstruction algorithm for single photon emission computed tomography with cone beam geometry," Int. J. of Imag. Sys. & Techn. **1**, 169–186 (1989).

[30]R. J. Jaszczak, R. E. Coleman, and F. R. Whitehead, "Physical factors affecting quantitative measurements using camera-based single photon emission computed tomography (SPECT)," IEEE Trans. Nucl. Sci. **28**, 69–80 (1981).

[31]J. W. Keyes, W. L. Rogers, N. H. Clinthorne, *et al.*, *Radioaktive isotope in Klinik und Furschung 15 Band*, edited by R. Hofer and H. Bergmann (Verlag, Vienna, 1982) Teil, pp. 529–537.

[32]A. E. Todd-Pokropek, *Radioaktive isotope in Klinik und Furschung 15 Band*, edited by R. Hofer and H. Bergmann (Verlag, Vienna, 1982) Teil, pp. 539–548.

[33]G. T. Gullberg, B. M. W. Tsui, C. R. Crawford, and E. R. Edgerton, "Estimation of geometrical parameters for fan beam tomography," Phy. Med. Biol. **32**, 1581–1594 (1987).

[34]D. W. Marquardt, "An algorithm for least-squares estimation of nonlinear parameters," SIAM **11**, 431–441 (1963).

[35]R. Deutsch, *Estimation Theory* (Prentice-Hall, Englewood Cliffs, New Jersey, 1965).

[36]W. Chang, S. Li, J. J. Williams, P. M. Bruch, C. A. Wesolowski, J. C. Ehrhardt, and P. T. Kirchner, "New methods of examining gamma camera collimators," J. Nucl. Med. **29**, 676–683 (1988).

[37]E. Busemann-Sokole, "Measurement of collimator hole angulation and camera head tilt for slant and parallel hole collimators used in SPECT," J. Nucl. Med. **28**, 1592–1598 (1987).

[38]M. D. Cerqueira, D. Matsuoka, J. L. Ritchie, and G. D. Harp, "The influence of collimators on SPECT center of rotation measurements: artifact generation and acceptance testing," J. Nucl. Med. **29**, 1393–1397 (1988).

[39]R. H. Huesman, G. T. Gullberg, W. L. Greenberg, T. F. Budinger, Users Manual—Donner Algorithms for Reconstruction Tomography, Lawrence Berkeley Laboratory Publication PUB-214, 1977.